

Two dimensional photonic crystals

Pi-Gang Luan and Zhen Ye

Wave Phenomena Laboratory, Department of Physics, National Central University, Chungli, Taiwan 32054
(October 27, 2018)

The topology, the symmetry involving the shape of dielectric cylinders, and the lattice structure are among the most important ingredients in the architecture of photonic crystals. In this paper, we present a systematic derivation of the formulas which are needed in computing the photonic band structures of many commonly used two dimensional lattice structures and dielectric cylinders with various kinds of symmetries and rotations. Further the results are applied to arrays of hollow cross-shaped cylinders embedded in the alumina ceramic background. A large complete photonic band gap is found in the high frequency regime.

PACS numbers: 41.10.Hv, 71.25.Cx, 43.20.+g.

I. INTRODUCTION

Over the past ten years, the propagation of classical waves in a periodic medium has attracted considerable interest. This includes electromagnetic (EM) wave propagation in periodic dielectric structures, and acoustic and elastic wave propagation in periodic elastic composites. A new research field emerges as the wave crystals including both photonic and sonic crystals. The photonic or sonic crystals respectively refer to crystal-like structures that modulate EM or acoustic wave propagation and thus lead to dispersion bands, in analogy with the electronic energy bands in solid state physics [1].

The research on photonic crystals has been particularly intensified, after the suggestion that photonic band gaps (PBG) could hinder spontaneous emission and block propagation of EM waves, thus providing the possibility to manipulate the propagation of EM waves [2,3]. Photonic crystals offer an unparalleled opportunity to design new optical devices and hold a great potential for many significant applications, such as semiconductor lasers and solar cells [2,4], high quality resonator and filters [5], controlling photon emission [6], optical fibers [7], guiding and bending of EM waves with minimum losses [8–10], single mode waveguides for light [11], low dimensional efficient transport of electrons and excitons by nanostructural networks [12], all polymer optoelectronic devices [13], semiconductor memory cells [14]. Many methods have been proposed for fabricating photonic crystals. These include square spiral microfabrication architecture for large three dimensional band gaps [15], filling the voids in titania with air by precipitation for the optical spectrum [16], using three dimensional carbon structures [17], large scale synthesis of silicon photonic crystals [18], fabrication of photonic crystals for visible spectrum by holographic lithography [19], the electrochemical techniques [20,21].

Indeed, the past a few years have witnessed rapid advances in both better understanding of the exquisite properties of photonic crystals and manipulation of EM waves by photonic crystals. A rich body of literature on photonic crystals exists and can be found on the internet [22]. Recently, scientists also investigated the spine from sea mouse [23]. They discovered that the spine consists of an array of regularly arranged hollow cylinders, and this simple structure gives rise to a spectacular iridescence. This is a remarkable example of photonic crystals by a living organism.

Although three dimensional (3D) photonic crystals suggest the most intriguing ideas for novel applications, two dimensional (2D) structures also find several unique uses [24], including the aforementioned waveguides and communication fibers [7,11] and the 2D periodic structures in living animals [23], feedback mirror in laser diodes [25] and so on. In addition, fabricating 3D periodic structures in the near infrared regime poses a significant challenge compared to the two dimensional situations [17,26–28]. Due to these reasons, the study of 2D photonic crystals has been overwhelmed in the last few years. The earliest theoretical analysis of 2D photonic band structure was done by Plihal et al. [29]. The experimental observation of photonic band structure in 2D periodic dielectric arrays was subsequently reported by Robertson et al. [30].

The important issue in the fabrication of photonic crystals is to create large, robust complete band gaps within which propagation of EM waves is prohibited in any direction. Several methods have been suggested for obtaining large complete band gaps in 2D situations. For example, it has been shown that large band gaps can be obtained by such as varying dielectric contrast ratio and filling factors, inserting a third component into the existing photonic crystals [31], reducing the structural symmetry [24], using non-circular rods [32,33] and subsequently by rotating

the non-circular rods [34,35], rotating the lattice structures [36], using anisotropic dielectric materials [37], using the effects of magnetic permeability [38], using metallic or metallodielectric rods [39–41], placing rods of various shapes on different lattice configurations such as square [29], triangular [37,42], honeycomb [24] and so on. Each approach may have its advantages and shortcomings. For example, the dielectric contrast is limited by material availability. The symmetry reduction and using non-circular rods may reduce the degeneracy of photonic bands at high symmetry points in the Brillouin zone, thus increasing band gaps. Although the metallic photonic crystals can yield large band gaps, they suffer from absorption. While the symmetry reduction method can enhance some high order band gaps, the low order gaps are often reduced [31]. Therefore each method has its own applicable situations.

Inspecting these progresses made towards better design of two dimensional photonic crystals, we realize that the topology, the symmetry involving the shape of dielectric cylinders, and the lattice structure are among the most important ingredients in the architecture of photonic crystals. The different combinations of these factors lead to applications for various purposes. We are therefore led to the task of deriving systematically necessary formulas computing band structures for various configurations. This paper is one of our attempts. In this paper, in an organized fashion we present the analytic results for computing the band structures of most commonly used lattice structures and dielectric cylinders with many kinds of symmetries and rotations. With the aim in mind that the reader can readily make use of these results, we summarize them in tables.

This paper is organized as follows. The general theory for EM waves in an arbitrary 2D periodic structures is presented in the next section. Using the plane wave expansion method, the secular equations are derived for determining the band structures for both E-polarization mode and H-polarization mode with the electric field and the magnetic field parallel to the longitudinal axis respectively. In the formulation, a structure factor is identified. Once this factor is known, the band structure can be computed by a standard diagonalization method. In section III, the structure factor is derived for a general configuration. Some common crystal structures with several rod shapes are considered in section IV. The results are presented in two tables. A numerical example is shown in section V, followed by concluding remarks in the last section where the extension to sonic crystals is also discussed.

II. THEORY

The photonic band structures can be obtained by solving Maxwell's equations using the plane-wave expansion method. This method can be referred to, for example, Refs. [29,34,43,44]. For the sake of convenience, we provide a brief account of this method. Consider a periodic array of dielectric cylinders. The longitudinal axes of the cylinders are along the z -axis. For dielectric materials, Maxwell's equations are represented in terms of the magnetic field \mathbf{H}

$$\nabla \times \left[\frac{1}{\epsilon(\mathbf{r})} \nabla \times \mathbf{H}(\mathbf{r}) \right] = \frac{\omega^2}{c_0^2} \mathbf{H}(\mathbf{r}), \quad (1)$$

where ϵ is the position-dependent dielectric constant, \mathbf{r} is the coordinates in the plane perpendicular to the rods, and c_0 is the EM wave phase speed in vacuum. By Bloch theorem [1], the magnetic field can be written as

$$\mathbf{H}(\mathbf{r}) = e^{i\mathbf{k}\cdot\mathbf{r}} \mathbf{H}_k(\mathbf{r}), \quad (2)$$

in which $\mathbf{H}_k(\mathbf{r})$ is a periodic function of the lattice structure, and \mathbf{k} is the Bloch wave vector within the first Brillouin zone.

Using the Fourier transformation, the magnetic field and the dielectric function can be expanded as,

$$\mathbf{H}_k(\mathbf{r}) = \sum_{\mathbf{G}} \sum_{j=1,2} \hat{e}_j H_{j,\mathbf{k}}(\mathbf{G}) e^{i\mathbf{G}\cdot\mathbf{r}}, \quad (3)$$

and

$$\epsilon(\mathbf{r}) = \sum_{\mathbf{G}} \epsilon(\mathbf{G}) e^{i\mathbf{G}\cdot\mathbf{r}}, \quad (4)$$

where \hat{e}_j is the base vector for the magnetic field, \mathbf{G} is a reciprocal lattice vector. Hereafter, all quantities with a hat refer to the unit vectors. For two dimensions, the E-polarization and H-polarization modes are decoupled. By taking Eqs. (2), (3), and (4) into Eq. (1), we obtain two eigen-equations

$$\sum_{\mathbf{G}'} |\mathbf{k} + \mathbf{G}| |\mathbf{k} + \mathbf{G}'| \epsilon^{-1}(\mathbf{G} - \mathbf{G}') H_{\perp,\mathbf{k}}(\mathbf{G}') = \frac{\omega^2}{c_0^2} H_{\perp,\mathbf{k}}(\mathbf{G}), \quad (5)$$

for the E-polarization and

$$\sum_{\mathbf{G}'} (\mathbf{k} + \mathbf{G}) \cdot (\mathbf{k} + \mathbf{G}') \epsilon^{-1}(\mathbf{G} - \mathbf{G}') H_{\parallel, \mathbf{k}}(\mathbf{G}') = \frac{\omega^2}{c_0^2} H_{\parallel, \mathbf{k}}(\mathbf{G}), \quad (6)$$

for the H-polarization. Here $\epsilon^{-1}(\mathbf{G} - \mathbf{G}')$ is the inverse matrix of $\epsilon(\mathbf{G} - \mathbf{G}')$, \perp and \parallel refer to the direction perpendicular and parallel to the z -axis. The Fourier components $\epsilon(\mathbf{G} - \mathbf{G}')$ is calculated as

$$\epsilon(\mathbf{G}) = \frac{1}{A} \int_A \epsilon(\mathbf{r}) e^{-i\mathbf{G} \cdot \mathbf{r}} d\mathbf{r}, \quad (7)$$

where the integration is performed over the area of one lattice unit cell, and A is the area.

For binary situations, Eq. (7) can be further simplified into

$$\epsilon(\mathbf{G}) = \begin{cases} f\epsilon_a + (1-f)\epsilon_b & \text{for } \mathbf{G} = 0, \\ (\epsilon_a - \epsilon_b)S(\mathbf{G}) & \text{for } \mathbf{G} \neq 0, \end{cases} \quad (8)$$

with ϵ_a and ϵ_b referring to the dielectric constants for the cylinders and background separately, and f is the filling factor defined as fraction of the area occupied by the cylinders in one unit cell. The factor $S(\mathbf{G})$ relies only on the geometry of the cylinders and the lattice structures, and is given by

$$S(\mathbf{G}) = \frac{1}{A} \int_{A_d} e^{-i\mathbf{G} \cdot \mathbf{r}} d\mathbf{r}, \quad (9)$$

where the integration is carried over the area occupied by the cylinders in the unit cell. We name $S(\mathbf{G})$ as the structure factor.

III. EVALUATION OF STRUCTURE FACTORS

It is clear from the above derivation that once the structure factor is known, the band structure for either the E-polarization or H-polarization modes can be readily evaluated by taking the structure factor into Eq. (8) and subsequently into Eqs. (5) and (6) respectively. In the following we evaluate the structure factor for common crystal structures.

A. Transformation of $S(\mathbf{G})$ under some operations

To proceed, first we discuss how the structure factor changes under certain operations with regard to a single cylinder. Different cylinders in a unit cell may undergo different operations. The final structure factor of the unit cell will be the sum of each individual structure factor. These operations include *translation*, *rotation*, *reflection* and *scaling* (*dilation* and *contraction*). Under these operations the new $S(\mathbf{G})$ is related to the original one by applying simple transformations. The knowledge of these transformations are useful in the calculation of the structure factor for various lattices.

1. Translation

In the $x - y$ plane, the translational operation is the simplest operation and it transforms the coordinates by a constant displacement \mathbf{r}_0 as

$$\mathbf{T}_t[\mathbf{r}] = \mathbf{r}' = \mathbf{r} + \mathbf{r}_0.$$

Under this operation, the structure factor changes as

$$\mathbf{T}_t[S(\mathbf{G})] = S' = e^{-i\mathbf{G} \cdot \mathbf{r}_0} S(\mathbf{G}). \quad (10)$$

2. Rotation

This operation rotates the cylinders by an angle θ . Since the calculation of structure factor must be coordinate independent, we can rotate the coordinate system by the same angle θ to simplify the calculation. In the new coordinates, the structure factor will be the same form as the original one. However, in the new system the vector \mathbf{G} is transformed as

$$\mathbf{T}_r \begin{pmatrix} G_x \\ G_y \end{pmatrix} = \begin{pmatrix} \cos \theta & \sin \theta \\ -\sin \theta & \cos \theta \end{pmatrix} \begin{pmatrix} G_x \\ G_y \end{pmatrix}, \quad (11)$$

where G_x and G_y are the \mathbf{G} components in the original coordinate system. Therefore under this operation, we have

$$\mathbf{T}_r[S(\mathbf{G})] = S(\mathbf{T}_r[\mathbf{G}]). \quad (12)$$

3. Reflection

The reflection operation is to reflect the system about a line. This operation will not change the form of the structure factor. Rather it just change the reciprocal vector. By analogy with the rotation operation, under the reflection operation we have

$$\mathbf{T}_{ref}[S(\mathbf{G})] = S(\mathbf{T}_{ref}[\mathbf{G}]). \quad (13)$$

4. Scaling

The scaling operation includes dilatation and contraction of the coordinates. Consider the operation

$$\mathbf{T}_s \begin{pmatrix} x \\ y \end{pmatrix} = \begin{pmatrix} x' \\ y' \end{pmatrix} = \begin{pmatrix} \lambda_x & 0 \\ 0 & \lambda_y \end{pmatrix} \begin{pmatrix} x \\ y \end{pmatrix} \quad (14)$$

Under this operation

$$\mathbf{T}_s[\mathbf{G} \cdot \mathbf{r}] = \mathbf{G} \cdot \mathbf{T}_s[\mathbf{r}] = \mathbf{T}_s[\mathbf{G}] \cdot \mathbf{r}, \quad (15)$$

and

$$dA \rightarrow \lambda_x \lambda_y dA. \quad (16)$$

From (15) and (16) we find

$$\mathbf{T}_s[S(\mathbf{G})] = \lambda_x \lambda_y S(\mathbf{T}_s[\mathbf{G}]). \quad (17)$$

5. The structure factors of circular and elliptic cylinders

As an example, we calculate the structure factors of a circular and an elliptic cylinder. The latter is considered as a result of the scaling operation on the former. For a circular cylinder of radius a , we have

$$S(\mathbf{G}) = \frac{2\pi a J_1(Ga)}{AG}. \quad (18)$$

For the elliptic rod, suppose the lengths of the principal axes (along x and y axes respectively) are a and b . According to the idea before, we can obtain the result by a scaling operation on the circular case. Here

$$\lambda_x = 1, \quad \lambda_y = \frac{b}{a}, \quad (19)$$

so

$$S(\mathbf{G}) = \frac{2\pi b J_1(\tilde{G}a)}{A\tilde{G}}, \quad (20)$$

where

$$\tilde{G} = \sqrt{G_x^2 + \left(\frac{b}{a}\right)^2 G_y^2}. \quad (21)$$

B. Structure factor of a polygonal cylinder

Now we consider the general case. Consider a polygonal cylinder with N sides. The N corners of the polygon are labeled as $\mathbf{r}_1, \mathbf{r}_2, \dots, \mathbf{r}_N$, where the j th corner $\mathbf{r}_j = (x_j, y_j)$, and we define $\mathbf{r}_{N+1} = \mathbf{r}_1$. Suppose we can find a vector field \mathbf{F} such that

$$(\nabla \times \mathbf{F})_z = e^{-i\mathbf{G} \cdot \mathbf{r}}, \quad (22)$$

then according to Stokes' Theorem, we have

$$\int_{A_d} \nabla \times \mathbf{F} \cdot d\mathbf{A} = \oint_{C_d} \mathbf{F} \cdot d\mathbf{r}, \quad d\mathbf{A} = dA\hat{z}, \quad (23)$$

and thus the original integral (9) is reduced to computing the line integral

$$I = \oint_{C_d} \mathbf{F} \cdot d\mathbf{r}, \quad (24)$$

where C_d is the boundary of the polygon. In the rest we present a detailed calculation of this line integration.

To begin with, assume $G_x \neq 0$. Choose

$$\mathbf{F} = F_y \hat{y}, \quad (25)$$

then solving the equation

$$(\nabla \times \mathbf{F})_z = \partial_x F_y = e^{-i\mathbf{G} \cdot \mathbf{r}} = e^{-iG_x x} e^{-iG_y y}$$

will gives us the solution

$$F_y = \frac{i}{G_x} e^{-i\mathbf{G} \cdot \mathbf{r}}. \quad (26)$$

The integral I now becomes

$$I = \frac{i}{G_x} \sum_{j=1}^N \int_{(x_j, y_j)}^{(x_{j+1}, y_{j+1})} e^{-i(G_x x + G_y y)} dy, \quad (27)$$

where $\int_{(x_j, y_j)}^{(x_{j+1}, y_{j+1})}$ denotes the line integral between j -th and $(j+1)$ -th corner, i.e., the j -th side. For the j -th side we have

$$\begin{aligned} & \int_{(x_j, y_j)}^{(x_{j+1}, y_{j+1})} e^{-i(G_x x + G_y y)} dy \\ &= \frac{i(y_{j+1} - y_j)(e^{-i\mathbf{G} \cdot \mathbf{r}_{j+1}} - e^{-i\mathbf{G} \cdot \mathbf{r}_j})}{\mathbf{G} \cdot (\mathbf{r}_{j+1} - \mathbf{r}_j)} \\ &= (y_{j+1} - y_j) e^{-i\mathbf{G} \cdot (\frac{\mathbf{r}_{j+1} + \mathbf{r}_j}{2})} \frac{\sin[\mathbf{G} \cdot (\frac{\mathbf{r}_{j+1} - \mathbf{r}_j}{2})]}{\mathbf{G} \cdot (\frac{\mathbf{r}_{j+1} - \mathbf{r}_j}{2})}. \end{aligned} \quad (28)$$

Substituting (28) into (27) and defining

$$\mathbf{C}_j \equiv \left(\frac{\mathbf{r}_{j+1} + \mathbf{r}_j}{2} \right), \quad \mathbf{S}_j \equiv \left(\frac{\mathbf{r}_{j+1} - \mathbf{r}_j}{2} \right), \quad (29)$$

$$\Delta y_j \equiv y_{j+1} - y_j, \quad (30)$$

we find

$$I = \sum_{j=1}^N \frac{i\Delta y_j e^{-i\mathbf{G} \cdot \mathbf{C}_j} \sin(\mathbf{G} \cdot \mathbf{S}_j)}{G_x \mathbf{G} \cdot \mathbf{S}_j}. \quad (31)$$

When $G_x = 0$, Eq.(31) no longer holds. We have to find another expression. In this case, since $G_y \neq 0$, we can choose

$$\mathbf{F} = F_x \hat{x} \quad (32)$$

and solve

$$(\nabla \times \mathbf{F})_z = -\partial_y F_x = e^{-iG_x x} e^{-iG_y y}$$

to find the solution

$$F_x = -\frac{i}{G_y} e^{-i\mathbf{G} \cdot \mathbf{r}}. \quad (33)$$

Taking this \mathbf{F} into Eq.(24) and defining

$$\Delta x_j \equiv x_{j+1} - x_j, \quad (34)$$

we find

$$I = \sum_{j=1}^N \frac{-i\Delta x_j e^{-i\mathbf{G} \cdot \mathbf{C}_j} \sin(\mathbf{G} \cdot \mathbf{S}_j)}{G_y \mathbf{G} \cdot \mathbf{S}_j}. \quad (35)$$

In fact, both (31) and (35) can be written in the unified expression

$$\begin{aligned} I &= \sum_{j=1}^N \frac{2i\mathbf{S}_j \cdot \hat{n}_2 e^{-i\mathbf{G} \cdot \mathbf{C}_j} \sin(\mathbf{G} \cdot \mathbf{S}_j)}{\mathbf{G} \cdot \hat{n}_1 \mathbf{G} \cdot \mathbf{S}_j} \\ &= \sum_{j=1}^N \frac{2i\hat{z} \cdot (\hat{n}_1 \times \mathbf{S}_j) e^{-i\mathbf{G} \cdot \mathbf{C}_j} \sin(\mathbf{G} \cdot \mathbf{S}_j)}{\mathbf{G} \cdot \hat{n}_1 \mathbf{G} \cdot \mathbf{S}_j}, \end{aligned} \quad (36)$$

where \hat{n}_1 is an arbitrary unit vector, and \hat{n}_2 is another unit vector defined by $\hat{n}_2 = \hat{z} \times \hat{n}_1$.

If we choose \hat{n}_1 as

$$\hat{n}_1 = \frac{\mathbf{G}}{G}, \quad (37)$$

where $G = |\mathbf{G}|$, we then obtain a general expression

$$I = \sum_{j=1}^N \frac{2i\hat{z} \cdot (\mathbf{G} \times \mathbf{S}_j) e^{-i\mathbf{G} \cdot \mathbf{C}_j} \sin(\mathbf{G} \cdot \mathbf{S}_j)}{G^2 \mathbf{G} \cdot \mathbf{S}_j}, \quad (38)$$

for either $G_x \neq 0$ or $G_y \neq 0$.

In the above we have obtained the general expression Eq. (38) of the integral I when $\mathbf{G} \neq 0$. Several remarks are worthwhile.

1. If $\mathbf{G} = 0$, the integral in (9) is simply A , i.e., the cross section area. However, we do not need to consider this situation because the structure factor at $\mathbf{G} = 0$ does not involve in the band structure calculation, referring to Eq. (8).
2. Formula (31), (35), (36) and (38) are still correct when the polygon region has several polygons. In this case the sum in (38) can be rewritten as

$$I = \sum_{p=1}^P \sum_{j_p=1}^{N_p} \frac{2i\hat{z} \cdot (\mathbf{G} \times \mathbf{S}_{j_p}) e^{-i\mathbf{G} \cdot \mathbf{C}_{j_p}} \sin(\mathbf{G} \cdot \mathbf{S}_{j_p})}{G^2 \mathbf{G} \cdot \mathbf{S}_{j_p}}, \quad (39)$$

where $p = 1, \dots, P$ and P is the total number of polygons; $j_p = 1, \dots, N_p$, with N_p being the total number of corners of the p -th polygon.

3. Since the integral (24) is calculated along a closed loop, we can always gauge transform the field \mathbf{F} by adding an arbitrary gradient:

$$\mathbf{F}' = \mathbf{F} + \nabla\Lambda, \quad (40)$$

where Λ is a scalar field. Under this gauge transformation, the structure factor is not changed. For example, denote \mathbf{F} in (26) as \mathbf{F}_1 and the \mathbf{F} in (33) as \mathbf{F}_2 , then

$$\mathbf{F}_1 - \mathbf{F}_2 = \nabla \left(\frac{-e^{-i\mathbf{G} \cdot \mathbf{r}}}{G_x G_y} \right). \quad (41)$$

Therefore \mathbf{F}_1 and \mathbf{F}_2 differs by a gradient, and both gave the same structure factor.

4. If $G_x = 0$, one can use Eq.(35); if $G_y = 0$, one can use Eq. (31). It can be proved that the result with $G_x = 0$ can also be obtained from Eq. (31) by taking the $G_x \rightarrow 0$ limit. Similarly, when $G_y = 0$, one can obtain the correct result from Eq. (31) by taking the $G_y \rightarrow 0$ limit.
5. For later convenience, we define a function $Q(x)$ as

$$Q(x) \equiv \frac{\sin x}{x}. \quad (42)$$

IV. SOME ANALYTIC EXAMPLES

Now we apply the above formulas to calculate explicitly the structure factors of various configurations.

A. Square lattice

First we consider the square lattice. The lattice constant is supposed to be d . The base vectors are

$$\mathbf{a}_1 = d\hat{x}, \quad \mathbf{a}_2 = d\hat{y}, \quad (43)$$

so the area of a unit cell is

$$A = d^2. \quad (44)$$

The bases of the reciprocal lattice are

$$\mathbf{b}_1 = \frac{2\pi}{d}\hat{x}, \quad \mathbf{b}_2 = \frac{2\pi}{d}\hat{y}, \quad (45)$$

which give

$$\mathbf{G} = n_1\mathbf{b}_1 + n_2\mathbf{b}_2 = \frac{2\pi}{d}(n_1\hat{x} + n_2\hat{y}), \quad (46)$$

or

$$G_x = \frac{2\pi n_1}{d}, \quad G_y = \frac{2\pi n_2}{d}. \quad (47)$$

1. *Square lattice with circular cylinders (SC)*

First we arrange the circular cylinders in the square lattice. This is simplest type of photonic crystals [29]. The radius of the cylinder is a . The structure factor is given by

$$S(\mathbf{G}) = 2f \frac{J_1(Ga)}{Ga}. \quad (48)$$

The filling fraction f and its maximum value f_{max} are

$$f = \frac{\pi a^2}{A} = \pi \left(\frac{a}{d}\right)^2, \quad f_{max} = \frac{\pi}{4}. \quad (49)$$

For a general (n_1, n_2) pair we have

$$Ga = \sqrt{\frac{4\pi^2 a^2}{d^2} (n_1^2 + n_2^2)} = \sqrt{4\pi f (n_1^2 + n_2^2)}. \quad (50)$$

2. *Square lattice with square cylinders (SS)*

Now we place the square cylinders on the square lattice [33]. The side length of the square is a . The structure factor is given by

$$S(\mathbf{G}) = fQ\left(\frac{G_x a}{2}\right)Q\left(\frac{G_y a}{2}\right) = fQ\left(\frac{n_1 \pi a}{d}\right)Q\left(\frac{n_2 \pi a}{d}\right). \quad (51)$$

Here the filling fraction and its maximum value are

$$f = \left(\frac{a}{d}\right)^2, \quad f_{max} = 1. \quad (52)$$

B. Triangular lattice

In this case we still assume the lattice constant l and circle radius a . The base vectors are given by

$$\mathbf{a}_1 = d\hat{x}, \quad \mathbf{a}_2 = d\left(\frac{1}{2}\hat{x} + \frac{\sqrt{3}}{2}\hat{y}\right), \quad (53)$$

so the area of a unit cell is

$$A = \frac{\sqrt{3}}{2} d^2. \quad (54)$$

The bases of the reciprocal lattice are

$$\mathbf{b}_1 = \frac{2\pi}{d}\left(\hat{x} - \frac{1}{\sqrt{3}}\hat{y}\right), \quad \mathbf{b}_2 = \frac{2\pi}{d}\frac{2}{\sqrt{3}}\hat{y}, \quad (55)$$

which give

$$\mathbf{G} = n_1 \mathbf{b}_1 + n_2 \mathbf{b}_2 = \frac{2\pi}{d}\left(n_1 \hat{x} + \frac{2n_2 - n_1}{\sqrt{3}} \hat{y}\right), \quad (56)$$

or

$$G_x = \frac{2\pi n_1}{d}, \quad G_y = \frac{2\pi}{d}\left(\frac{2n_2 - n_1}{\sqrt{3}}\right). \quad (57)$$

1. *Triangular lattice with circular cylinder (TC)*

This is the case considered by [42]. The radius of the circle is a . The structure factor is

$$S = \frac{I}{A} = 2f \frac{J_1(Ga)}{Ga}, \quad (58)$$

with

$$f = \frac{\pi a^2}{A} = \frac{2\pi}{\sqrt{3}} \left(\frac{a}{d}\right)^2, \quad f_{max} = \frac{\pi}{2\sqrt{3}}. \quad (59)$$

For a general (n_1, n_2) pair we have

$$\begin{aligned} Ga &= \sqrt{\frac{16\pi^2 a^2}{3d^2} (n_1^2 + n_2^2 - n_1 n_2)} \\ &= \sqrt{\frac{8\pi f}{\sqrt{3}} (n_1^2 + n_2^2 - n_1 n_2)}. \end{aligned} \quad (60)$$

2. *Triangular lattice with hexagonal cylinder (TH)*

In this case we assume the hexagon side length is a , thus the cross section area is

$$A = \frac{3\sqrt{3}a^2}{2}. \quad (61)$$

The filling fraction is given by

$$f = \frac{A}{A} = 3 \left(\frac{a}{d}\right)^2, \quad (62)$$

with maximum value

$$f_{max} = \frac{3}{4}. \quad (63)$$

The structure factor is

$$S(\mathbf{G}) = \frac{(2f/3)}{G_x a} \left\{ \sin \left[\frac{(3G_x + \sqrt{3}G_y)a}{4} \right] Q \left[\frac{(G_x - \sqrt{3}G_y)a}{4} \right] + \sin \left[\frac{(3G_x - \sqrt{3}G_y)a}{4} \right] Q \left[\frac{(G_x + \sqrt{3}G_y)a}{4} \right] \right\} \quad (64)$$

or

$$S(\mathbf{G}) = \frac{(fd/3)}{n_1 \pi a} \left\{ \sin \left[\frac{(n_1 + n_2)\pi a}{d} \right] Q \left[\frac{(n_1 - n_2)\pi a}{d} \right] + \sin \left[\frac{(2n_1 - n_2)\pi a}{d} \right] Q \left[\frac{n_2 \pi a}{d} \right] \right\}. \quad (65)$$

C. Tables of structure factors

In this section we consider various arrangements of rod cross section and lattices. Eighteen patterns (configurations) are illustrated in Fig. (1) and (2). Here we consider square, triangular, and honeycomb lattices. The abbreviation of these patterns are defined in the figure captions. For example, TC refers to the situation that circular cylinders are arranged in a triangular lattice. For a circular rod the parameter a denotes the radius of cylinder. For a polygonal cylinder, a represents the side length. For a “cross”-shaped or a “rotated cross”-shaped rod, a and aa represent the “long” and “short” side lengths of the corresponding rectangle. In a unit cell of the “triangular-diamonds” or “triangular-rotated diamonds” pattern (See Figs. 2(j) and (k)) there are three “diamonds”. In the “rotated diamonds”

pattern the distance between the center of each diamond and the center of unit cell is chosen to be $d/4$; d is the lattice constant.

The crystal structures shown by these two figures are most common in photonic design. While some have already been published, many are reported for the first time. In the next section, a new class of photonic crystals will be investigated. The corresponding band structure will be computed. The corresponding properties and the forms of unit cells are given in Table I, and the structure factors are listed in Table II, respectively. In these tables, the first column refers to the combination of the lattice structure and the shape of rods, the second to the unit cells, the third to the filling factor formula, with the maximum value being listed in the fourth column. The next two columns refer to the two base reciprocal vectors.

V. THE NUMERICAL RESULTS

In this section we consider the band structure of the 2D photonic crystals made by drilling hollow cross-shaped cylinders in an alumina ceramic background and by placing cross-shaped alumina ceramic cylinders in the air. The cross-shaped cylinders are arranged in a square lattice configuration, corresponding to Fig. 1(d). The following parameters are used: filling factor $f = 0.5$, the ratio between b and a is 0.3. The dielectric constant of the alumina ceramic is 8.9. We used more than 600 plane waves. The inaccuracy is less than 1%.

The photonic band structures are plotted in Fig. 3. Here we see from (a) that an absolute band gap appears in the high frequency range for the E- and H- polarizations, in the case of air cylinders in the dielectric medium. Incidentally, the absolute band gap position is at around the same regime as in [45] and [46]; we note that in [45], it was the very high dielectric cylinders that are placed in air. This indicates that it is relatively easy to obtain the absolute band gap in the infrared regime with this type of photonic crystals. We also see that there are more complete gaps in the E-polarization mode than in the H-mode. These occur at around $\omega d/(2\pi c) = 0.25, 0.6$, but the largest gap happens at the position of the absolute gap around $\omega d/(2\pi c) = 0.7$, where the gap of the H-polarization is wider than that of the E-polarization. In the opposite case where the cylinders are made of high dielectric constant materials, there is no absolute band gap at all. In fact, there is no gap for the E-polarization. However, a complete gap appears around $\omega d/(2\pi c) = 0.35$ for the H-polarization.

VI. SUMMARY

In this article, we derived necessary formulas needed for computing the band structures of various types of photonic crystals. The results are systematically presented in tables, so that the reader could easily make a use of them. As an example, we applied the results to two dimensional arrays of hollow cross-shaped cylinders embedded in an alumina ceramic medium. For this new class of photonic crystals, a large absolute photonic band gap is discovered in the high frequency region.

Finally, we want to make a connection between the photonic and sonic crystals. In the acoustic case, the wave equation is governed by

$$\nabla \cdot \left(\frac{1}{\rho(\mathbf{r})} \nabla p(\mathbf{r}) \right) + \frac{\omega^2}{\rho(\mathbf{r})c^2(\mathbf{r})} p(\mathbf{r}) = 0. \quad (66)$$

In the H-polarization mode, Maxwell equation is from Eq. (1)

$$\nabla \cdot \left(\frac{1}{\epsilon(\mathbf{r})} \nabla H_{\parallel}(\mathbf{r}) \right) + \frac{\omega^2}{\epsilon(\mathbf{r})c^2(\mathbf{r})} H_{\parallel}(\mathbf{r}) = 0, \quad (67)$$

where $c^2 = c_0^2/\epsilon(\mathbf{r})$. Therefore the acoustic pressure field and the magnetic field have an one-to-one correspondence given by the following mapping,

$$\rho(\mathbf{r}) \rightleftharpoons \epsilon(\mathbf{r}), \quad \rho(\mathbf{r})c^2(\mathbf{r}) \rightleftharpoons \epsilon(\mathbf{r})c^2(\mathbf{r}). \quad (68)$$

ACKNOWLEDGMENTS

This work received support from the National Science Council.

- [1] e. g. C. Kittel, *Introduction to solid state physics* (John Wiley & Sons, New York, 1996).
- [2] E. Yablonovitch, Phys. Rev. Lett. **58**, 2059 (1987).
- [3] S. John, Phys. Rev. Lett. **58**, 2486 (1987).
- [4] O. Painter, *et al.*, Science **284**, 1819 (1999).
- [5] R. D. Meade, *et al.*, Phys. Rev. B **44** 13772 (1991).
- [6] S. Noda, A. Chutinan, and M. Imada, Nature **407**, 608 (2000).
- [7] J. C. Knight, J. Broeng, T. A. Birks, P. St. J. Russell, Science **282**, 1476 (1998).
- [8] S. Y. Lin, E. Chow, V. Hietala, P. R. Villeneuve, J. D. Joannopoulos, Science **282**, 274 (1998).
- [9] J. S. Foresi, *et al.*, Nature **390**, 143 (1997).
- [10] E. Chow, *et al.*, Nature **407**, 983 (2000).
- [11] R. F. Cregan, *et al.*, Science **285**, 1537 (1999).
- [12] Y. Huang, X. Duan, Q. Wei, and C. M. Lieber, Science **291**, 630 (2001).
- [13] P. K. H. Ho, D. S. Thomas, R. H. Friend, N. Tessler, Science **285**, 233 (1999).
- [14] S. Zimmermann, A. Wixforth, J. P. Kottaus, W. Wegscheider, M. Bichler, Science **283**, 1292 (1999).
- [15] O. Toader and S. John, Science **292**, 1133 (2001).
- [16] J. E. G. J. Wijnhoven and W. L. Vos, Science **281**, 802 (1998).
- [17] A. Zakhidov *et al.*, Science **282**, 897 (1998).
- [18] A. Blanco, *et al.*, Nature **405**, 437 (2000).
- [19] M. Campbell, *et al.*, Nature **404**, 53 (2000).
- [20] F. J. P. Schuurmanns, D. Vanmaekelbergh, J. van de Lagemaat, and A. Lagendijk, Science **284**, 141 (1999).
- [21] P. V. Braun and P. Wiltzius, Nature **402**, 603 (1999).
- [22] <http://www.home.earthlink.net/~jpdowling/pbgbib.html>.
- [23] A. R. Parker, R. C. McPhedran, D. R. McKenzie, L. C. Botten, N. P. Nicorvici, Nature **409**, 36 (2001).
- [24] C. M. Anderson and K. P. Giapis, Phys. Rev. Lett. **77**, 2949 (1996).
- [25] D. L. Bullock, C. Shih, and R. S. Margulies, J. Opt. Soc. Am. **B10**, 399 (1993).
- [26] S. Y. Lin, *et al.*, Nature **394**, 251 (1998).
- [27] T. F. Krauss, R. De La Rue, and S. Band, Nature **383**, 699 (1996)
- [28] H. B. Lin, R. J. Tonucci, and J. Campillo, Appl. Phys. Lett. **68**, 2927 (1996).
- [29] M. Plihal, A. Shambrook, A. A. Maradudin, and P. Sheng, Opt. Comm. **80**, 199 (1991).
- [30] W. M. Robertson, G. Arjavalingam, R. D. Meade, K. D. Brommer, A. M. Rappe, and J. D. Joannopoulos, Phys. Rev. Lett. **68**, 2023 (1992).
- [31] X. Zhang, *et al.*, Phys. Rev. B **61**, 1892 (2000).
- [32] R. Padjen, J. M. Gerard, and J. Y. Marzin, J. Mod. Opt. **41**, 295 (1994).
- [33] P. R. Villeneuve and M. Piche, Phys. Rev. B **46**, 4973 (1992).
- [34] X. H. Wang, B. Y. Gu, Z. Y. Li, and G. Z. Yang, Phys. Rev. B **60**, 11417 (1999).
- [35] M. Agio and L. C. Andreani, Phys. Rev. B **61**, 15519 (2000).
- [36] C. M. Anderson and K. P. Giapis, Phys. Rev. B **56**, 7313 (1997).
- [37] Z. Y. Li, B. Y. Gu, and G. Z. Yang, Phys. Rev. Lett. **81**, 2574 (1998).
- [38] M. M. Sigalas, C. M. Soukoulis, R. Biswas, and K. M. Ho, Phys. Rev. B **56**, 959 (1997).
- [39] N. A. Nicorvici, R. C. McPhedran, and L. C. Botten, Phys. Rev. B **52**, 1135 (1995).
- [40] D. F. Sievenpiper, *et al.*, Phys. Rev. Lett. **80**, 2829 (1998).
- [41] K. A. McIntosh *et al.*, Appl. Phys. Lett. **70**, 2937 (1997).
- [42] e. g. M. Plihal and A. A. Maradudin, Phys. Rev. **44**, 8565 (1991).
- [43] K. M. Ho, C. T. Chan, and C. M. Soukoulis, Phys. Rev. Lett. **65**, 3152 (1990).
- [44] K. M. Leung and Y. F. Liu, Phys. Rev. Lett. **65**, 2646 (1990).
- [45] C. S. Lee and H. Y. Park, Phys. Rev. **E56**, R6291 (1997).
- [46] X. Zhang and Z. Q. Zhang, Phys. Rev. **B61**, 9847 (2000).

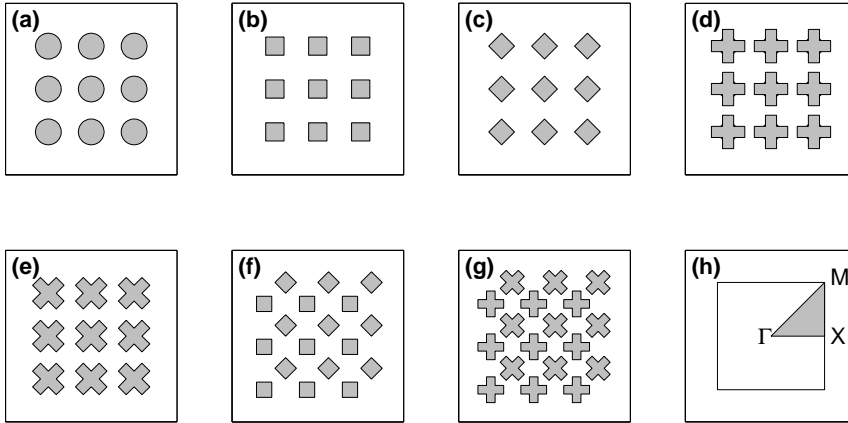


FIG. 1. Patterns of the square lattice. (a) square-circle (SC). (b) square-square (SS). (c) square-rotated square (SRS). (d) square-cross (SCR). (e) square-rotated cross (SRCR). (f) square-mixed square (SMS). (g) square-mixed cross (SMCR). (h) The first Brillouin zone of square lattice. The band structure is calculated along the boundary $M - \Gamma - X - M$ of the gray region.

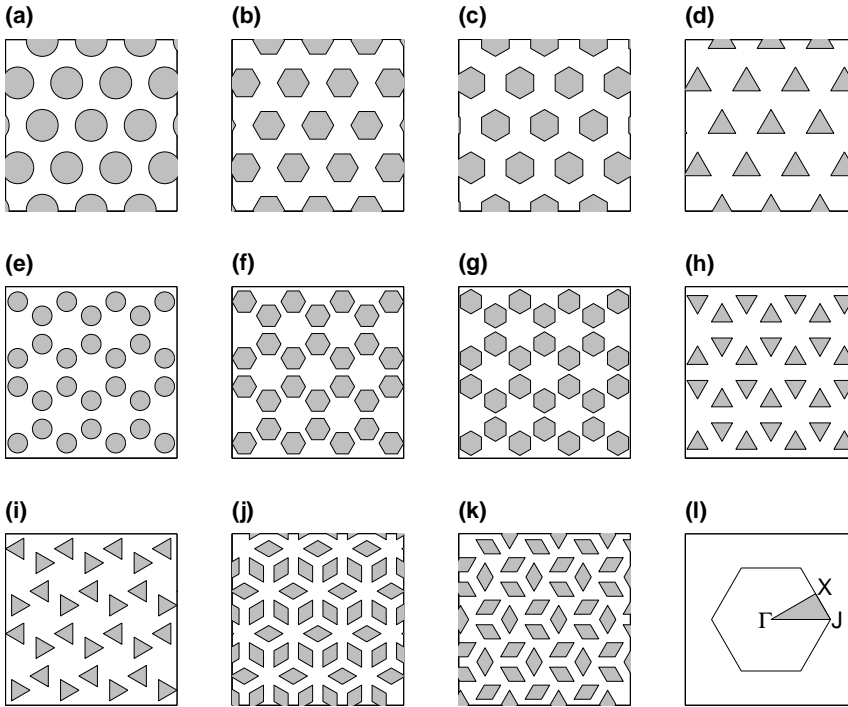


FIG. 2. Patterns of the triangular lattice. (a) triangular-circle (TC). (b) triangular-hexagon (TH). (c) triangular-rotated hexagon (TRH). (d) triangular-triangle (TT). (e) honeycomb-circle (HC). (f) honeycomb-hexagon (HH). (g) honeycomb-rotated hexagon (HRH). (h) honeycomb-triangle (HT). (i) honeycomb-rotated triangle (HRT). (j) triangular-diamonds (TD). (k) triangular-rotated diamonds (TRD). (l) The first Brillouin zone of triangular lattice. The band structure is calculated along the boundary $X - \Gamma - J - X$ of the gray region.

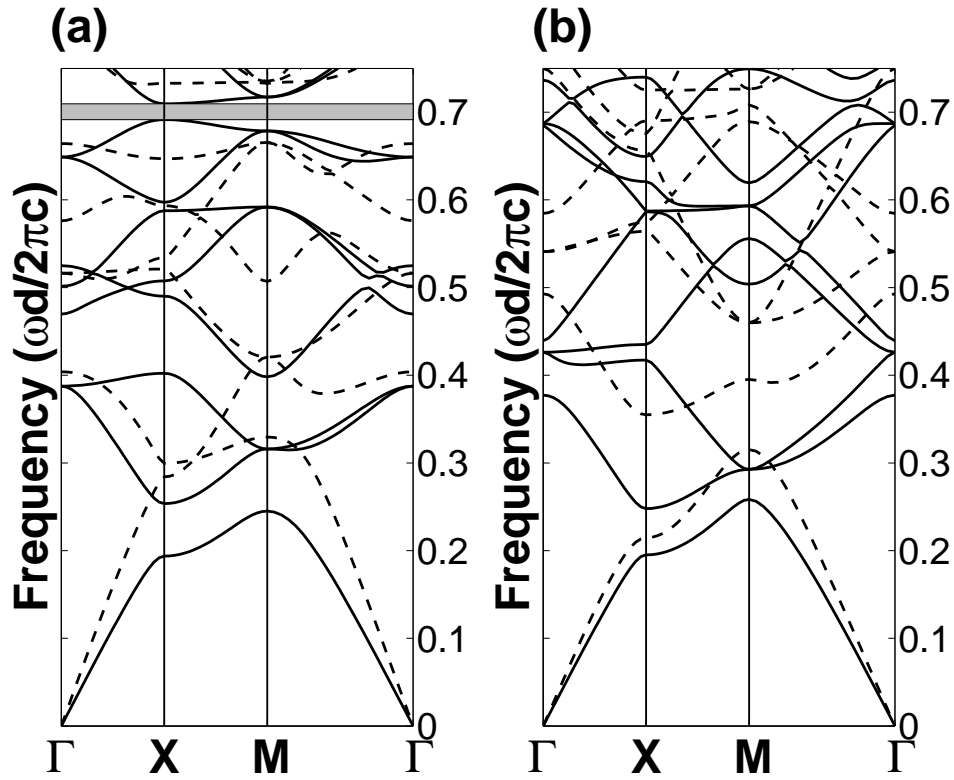


FIG. 3. The photonic band structures. The solid and dashed lines refer to the E-polarization and H-polarization modes respectively. (a) Air cylinders in alumina ceramics. The shaded area denotes the complete band gap. (b) Alumina ceramics cylinders in air.

TABLE I. Properties of various patterns

\square latt.	Unit cell	f	f_{max}	G_x	G_y
SC		$\frac{\pi a^2}{d^2}$	$\frac{\pi}{4}$	$\frac{2\pi n_1}{d}$	$\frac{2\pi n_2}{d}$
SS		$\frac{a^2}{d^2}$	1	$\frac{2\pi n_1}{d}$	$\frac{2\pi n_2}{d}$
SRS		$\frac{a^2}{d^2}$	$\frac{1}{2}$	$\frac{2\pi n_1}{d}$	$\frac{2\pi n_2}{d}$
SCR		$\frac{\alpha(2-\alpha)a^2}{d^2}$	$\alpha(2-\alpha)$	$\frac{2\pi n_1}{d}$	$\frac{2\pi n_2}{d}$
SRCR		$\frac{\alpha(2-\alpha)a^2}{d^2}$	$\frac{2\alpha(2-\alpha)}{(1+\alpha)^2}$	$\frac{2\pi n_1}{d}$	$\frac{2\pi n_2}{d}$
SMS		$\frac{2a^2}{d^2}$	$4(3-2\sqrt{2})$	$\frac{2\pi n_1}{d}$	$\frac{2\pi n_2}{d}$
SMCR		$\frac{2\alpha(2-\alpha)a^2}{d^2}$	$\frac{4\alpha(2-\alpha)}{[(\sqrt{2}+1)\alpha+1]^2}$ if $\alpha \leq \sqrt{2}-1$ $\frac{8\alpha(2-\alpha)}{[\alpha+(\sqrt{2}+1)]^2}$ if $\alpha > \sqrt{2}-1$	$\frac{2\pi n_1}{d}$	$\frac{2\pi n_2}{d}$
\triangle latt.	Unit cell	f	f_{max}	G_x	G_y
TC		$\frac{2\pi a^2}{\sqrt{3}d^2}$	$\frac{\pi}{2\sqrt{3}}$	$\frac{2\pi n_1}{d}$	$\frac{2\pi(2n_2-n_1)}{\sqrt{3}d}$
TH		$\frac{3a^2}{d^2}$	$\frac{3}{4}$	$\frac{2\pi n_1}{d}$	$\frac{2\pi(2n_2-n_1)}{\sqrt{3}d}$
TRH		$\frac{3a^2}{d^2}$	1	$\frac{2\pi n_1}{d}$	$\frac{2\pi(2n_2-n_1)}{\sqrt{3}d}$
TT		$\frac{a^2}{2d^2}$	$\frac{1}{2}$	$\frac{2\pi n_1}{d}$	$\frac{2\pi(2n_2-n_1)}{\sqrt{3}d}$
HC		$\frac{4\pi a^2}{\sqrt{3}d^2}$	$\frac{\pi}{3\sqrt{3}}$	$\frac{2\pi n_1}{d}$	$\frac{2\pi(2n_2-n_1)}{\sqrt{3}d}$
HH		$\frac{6a^2}{d^2}$	$\frac{2}{3}$	$\frac{2\pi n_1}{d}$	$\frac{2\pi(2n_2-n_1)}{\sqrt{3}d}$
HRH		$\frac{6a^2}{d^2}$	$\frac{1}{2}$	$\frac{2\pi n_1}{d}$	$\frac{2\pi(2n_2-n_1)}{\sqrt{3}d}$
HT		$\frac{a^2}{d^2}$	1	$\frac{2\pi n_1}{d}$	$\frac{2\pi(2n_2-n_1)}{\sqrt{3}d}$
HRT		$\frac{a^2}{d^2}$	$\frac{3}{4}$	$\frac{2\pi n_1}{d}$	$\frac{2\pi(2n_2-n_1)}{\sqrt{3}d}$
TD		$\frac{3a^2}{d^2}$	1	$\frac{2\pi n_1}{d}$	$\frac{2\pi(2n_2-n_1)}{\sqrt{3}d}$
TRD		$\frac{3a^2}{d^2}$	$\frac{3}{4}$	$\frac{2\pi n_1}{d}$	$\frac{2\pi(2n_2-n_1)}{\sqrt{3}d}$

TABLE II. Structure Factors for Square and Triangular Lattices

\square latt.	$S(\mathbf{G})$
SC	$2f \frac{J_1(Ga)}{Ga}$
SS	$fQ\left(\frac{G_x a}{2}\right)Q\left(\frac{G_y a}{2}\right)$
SRS	$fQ\left(\frac{(G_x+G_y)a}{2\sqrt{2}}\right)Q\left(\frac{(G_x-G_y)a}{2\sqrt{2}}\right)$
SCR	$\frac{f}{2-\alpha} \left[Q\left(\frac{G_x a}{2}\right)Q\left(\frac{G_y b}{2}\right) + Q\left(\frac{G_x b}{2}\right)Q\left(\frac{G_y a}{2}\right) - \alpha Q\left(\frac{G_x b}{2}\right)Q\left(\frac{G_y b}{2}\right) \right]$
SRCR	$\frac{f}{2-\alpha} \left[Q\left(\frac{(G_x+G_y)a}{2\sqrt{2}}\right)Q\left(\frac{(G_x-G_y)b}{2\sqrt{2}}\right) + Q\left(\frac{(G_x+G_y)b}{2\sqrt{2}}\right)Q\left(\frac{(G_x-G_y)a}{2\sqrt{2}}\right) - \alpha Q\left(\frac{(G_x+G_y)b}{2\sqrt{2}}\right)Q\left(\frac{(G_x-G_y)b}{2\sqrt{2}}\right) \right]$
SMS	$\frac{f}{2} \left[Q\left(\frac{G_x a}{2}\right)Q\left(\frac{G_y a}{2}\right) + (-1)^{n_1+n_2} Q\left(\frac{(G_x+G_y)a}{2\sqrt{2}}\right)Q\left(\frac{(G_x-G_y)a}{2\sqrt{2}}\right) \right]$
SMCR	$\frac{f}{2(2-\alpha)} \left\{ \left[Q\left(\frac{G_x a}{2}\right)Q\left(\frac{G_y b}{2}\right) + Q\left(\frac{G_x b}{2}\right)Q\left(\frac{G_y a}{2}\right) - \alpha Q\left(\frac{G_x b}{2}\right)Q\left(\frac{G_y b}{2}\right) \right] + (-1)^{n_1+n_2} \left[Q\left(\frac{(G_x+G_y)a}{2\sqrt{2}}\right)Q\left(\frac{(G_x-G_y)b}{2\sqrt{2}}\right) + Q\left(\frac{(G_x+G_y)b}{2\sqrt{2}}\right)Q\left(\frac{(G_x-G_y)a}{2\sqrt{2}}\right) - \alpha Q\left(\frac{(G_x+G_y)b}{2\sqrt{2}}\right)Q\left(\frac{(G_x-G_y)b}{2\sqrt{2}}\right) \right] \right\}$
\triangle latt.	$S(\mathbf{G})$
TC	$2f \frac{J_1(Ga)}{Ga}$
TH	$\frac{2f}{3G_x a} \left\{ \sin\left[\frac{(3G_x-\sqrt{3}G_y)a}{4}\right] Q\left[\frac{(G_x+\sqrt{3}G_y)a}{4}\right] + \sin\left[\frac{(3G_x+\sqrt{3}G_y)a}{4}\right] Q\left[\frac{(G_x-\sqrt{3}G_y)a}{4}\right] \right\}$
TH($G_x = 0$)	$\frac{2f}{3\left(\frac{\sqrt{3}G_y a}{2}\right)^2} \left[1 - \cos\left(\frac{\sqrt{3}G_y a}{2}\right) + \frac{\sqrt{3}G_y a}{2} \sin\left(\frac{\sqrt{3}G_y a}{2}\right) \right]$
TRH	$\frac{2f}{3G_y a} \left\{ \sin\left[\frac{(\sqrt{3}G_x+3G_y)a}{4}\right] Q\left[\frac{(\sqrt{3}G_x-G_y)a}{4}\right] - \sin\left[\frac{(\sqrt{3}G_x-3G_y)a}{4}\right] Q\left[\frac{(\sqrt{3}G_x+G_y)a}{4}\right] \right\}$
TRH($G_y = 0$)	$\frac{2f}{3\left(\frac{\sqrt{3}G_x a}{2}\right)^2} \left[1 - \cos\left(\frac{\sqrt{3}G_x a}{2}\right) + \frac{\sqrt{3}G_x a}{2} \sin\left(\frac{\sqrt{3}G_x a}{2}\right) \right]$
TT	$\frac{2if \exp\left(\frac{-iG_y a}{4\sqrt{3}}\right)}{G_x a} \left\{ e^{-\frac{iG_x a}{4}} Q\left[\frac{(G_x-\sqrt{3}G_y)a}{4}\right] - e^{\frac{iG_x a}{4}} Q\left[\frac{(G_x+\sqrt{3}G_y)a}{4}\right] \right\}$
TT($G_x = 0$)	$\frac{2f \exp\left(\frac{iG_y a}{2\sqrt{3}}\right)}{\left(\frac{\sqrt{3}G_y a}{2}\right)} \left(1 - i\frac{\sqrt{3}G_y a}{2} - e^{-i\frac{\sqrt{3}G_y a}{2}} \right)$
HC	$2f \cos\left[\frac{(n_1+n_2)\pi}{3}\right] \left(\frac{J_1(Ga)}{Ga}\right)$
HH	$\frac{2f \cos\left[\frac{(n_1+n_2)\pi}{3}\right]}{3G_x a} \left\{ \sin\left[\frac{(3G_x-\sqrt{3}G_y)a}{4}\right] Q\left[\frac{(G_x+\sqrt{3}G_y)a}{4}\right] + \sin\left[\frac{(3G_x+\sqrt{3}G_y)a}{4}\right] Q\left[\frac{(G_x-\sqrt{3}G_y)a}{4}\right] \right\}$
HH($G_x = 0$)	$\frac{2f \cos\left[\frac{(n_1+n_2)\pi}{3}\right]}{3\left(\frac{\sqrt{3}G_y a}{2}\right)^2} \left[1 - \cos\left(\frac{\sqrt{3}G_y a}{2}\right) + \frac{\sqrt{3}G_y a}{2} \sin\left(\frac{\sqrt{3}G_y a}{2}\right) \right]$
HRH	$\frac{2f \cos\left[\frac{(n_1+n_2)\pi}{3}\right]}{3G_y a} \left\{ \sin\left[\frac{(\sqrt{3}G_x+3G_y)a}{4}\right] Q\left[\frac{(\sqrt{3}G_x-G_y)a}{4}\right] - \sin\left[\frac{(\sqrt{3}G_x-3G_y)a}{4}\right] Q\left[\frac{(\sqrt{3}G_x+G_y)a}{4}\right] \right\}$
HRH($G_y = 0$)	$\frac{2f \cos\left[\frac{(n_1+n_2)\pi}{3}\right]}{3\left(\frac{\sqrt{3}G_x a}{2}\right)^2} \left[1 - \cos\left(\frac{\sqrt{3}G_x a}{2}\right) + \frac{\sqrt{3}G_x a}{2} \sin\left(\frac{\sqrt{3}G_x a}{2}\right) \right]$
HT	$\frac{2f}{G_x a} \left\{ \sin\left[\frac{(\sqrt{3}G_x-G_y)a}{4\sqrt{3}} + \frac{(n_1+n_2)\pi}{3}\right] Q\left[\frac{(G_x+\sqrt{3}G_y)a}{4}\right] + \sin\left[\frac{(\sqrt{3}G_x+G_y)a}{4\sqrt{3}} - \frac{(n_1+n_2)\pi}{3}\right] Q\left[\frac{(G_x-\sqrt{3}G_y)a}{4}\right] \right\}$
HT($G_x = 0$)	$\frac{2f}{\left(\frac{\sqrt{3}G_y a}{2}\right)^2} \left\{ \cos\left[\frac{G_y a}{2\sqrt{3}} + \frac{(n_1+n_2)\pi}{3}\right] + \frac{\sqrt{3}G_y a}{2} \sin\left[\frac{G_y a}{2\sqrt{3}} + \frac{(n_1+n_2)\pi}{3}\right] - \cos\left[\frac{G_y a}{\sqrt{3}} - \frac{(n_1+n_2)\pi}{3}\right] \right\}$
HRT	$\frac{2f}{G_y a} \left\{ \sin\left[\frac{(G_x+\sqrt{3}G_y)a}{4\sqrt{3}} - \frac{(n_1+n_2)\pi}{3}\right] Q\left[\frac{(\sqrt{3}G_x-G_y)a}{4}\right] - \sin\left[\frac{(G_x-\sqrt{3}G_y)a}{4\sqrt{3}} - \frac{(n_1+n_2)\pi}{3}\right] Q\left[\frac{(\sqrt{3}G_x+G_y)a}{4}\right] \right\}$
HRT($G_y = 0$)	$\frac{2f}{\left(\frac{\sqrt{3}G_x a}{2}\right)^2} \left\{ \cos\left[\frac{G_x a}{2\sqrt{3}} + \frac{(n_1+n_2)\pi}{3}\right] - \cos\left[\frac{G_x a}{\sqrt{3}} - \frac{(n_1+n_2)\pi}{3}\right] + \frac{\sqrt{3}G_x a}{2} \sin\left[\frac{G_x a}{2\sqrt{3}} + \frac{(n_1+n_2)\pi}{3}\right] \right\}$
TD	$\frac{f}{3} \left\{ e^{-i\frac{(2n_2-n_1)\pi}{3}} Q\left[\frac{(\sqrt{3}G_x+G_y)a}{4}\right] Q\left[\frac{(\sqrt{3}G_x-G_y)a}{4}\right] + e^{i\frac{(n_1+n_2)\pi}{3}} Q\left(\frac{G_y a}{2}\right) Q\left[\frac{(\sqrt{3}G_x-G_y)a}{4}\right] + e^{-i\frac{(2n_1-n_2)\pi}{3}} Q\left(\frac{G_y a}{2}\right) Q\left[\frac{(\sqrt{3}G_x+G_y)a}{4}\right] \right\}$
TRD	$\frac{f}{3} \left\{ i^{-n_1} Q\left[\frac{(G_x+\sqrt{3}G_y)a}{4}\right] Q\left[\frac{(G_x-\sqrt{3}G_y)a}{4}\right] + i^{(n_1-n_2)} Q\left(\frac{G_x a}{2}\right) Q\left[\frac{(G_x+\sqrt{3}G_y)a}{4}\right] + i^{n_2} Q\left(\frac{G_x a}{2}\right) Q\left[\frac{(G_x-\sqrt{3}G_y)a}{4}\right] \right\}$